(N-C_nH_{2n-1})-1,3-Azapropanedithiolate (n = 5, 6, 7)-bridged diiron complexes as mimics for the active site of [FeFe]-hydrogenases: the influence of the bridge on the diiron complex†

Youtao Si,[ab] Chengbing Ma,[a] Mingqiang Hu,[ab] Hui Chen,[a] Changneng Chen*[a] and Qiutian Liu[a]

Received (in Durham, UK) 7th November 2006, Accepted 28th March 2007
First published as an Advance Article on the web 24th April 2007
DOI: 10.1039/b616236c

To further understand the effects of 1,3-azadithiolate (ADT) bridges on the structures and properties of diiron complexes, a novel family of (N-C_nH_{2n-1})-1,3-azapropanedithiolate-bridged diiron complexes [$Fe_2(CO)_6(CH_2S)_2N$–C_nH_{2n-1}] (n = 5, 6, 7) and their PMe_3-disubstituted complexes [$Fe_2(CO)_4(PMe_3)_2(CH_2S)_2N$–$C_nH_{2n-1}$] ($n$ = 5, 6, 7) were synthesized as mimics of [FeFe]-hydrogenases. Our studies suggest that the coordination configurations, CO stretching frequencies, ^1H and ^{31}P NMR signals, redox potentials and electrocatalytic H_2-production processes of diiron complexes are closely pertinent to the electron-donating abilities and steric chemistry of the ADT bridges.

Introduction

Hydrogenases are enzymes adept at catalyzing the oxidation of molecular hydrogen or its production from protons and electrons.[1] According to the metals included in the enzymes, organometallic hydrogenases are generally divided into three major classes: [FeFe]-hydrogenases, [NiFe]-hydrogenases and the newly known [Fe]-hydrogenases.[2,3] [FeFe]-hydrogenases are more O_2 sensitive and committed to more efficient H_2 production than [NiFe]-hydrogenases.[4] It is the significant ability of [FeFe]-hydrogenases that inspires many chemists seeking active hydrogen production catalysts to synthesize mimics of its active site.[5–11] X-Ray crystallographic studies on [FeFe]-hydrogenases isolated from *Clostridium pasteurianum* and *Desulfovibrio desulfuricans* have suggested that the active site is composed of a "butterfly" diiron unit that is linked to a typical Fe_4S_4 cuboidal subcluster by a cysteine-S residue.[12–14] The dithiolate bridge between the two iron atoms of the 2Fe2S cluster has recently been suggested to be an azadithiolate, SCH_2NHCH_2S (ADT),[12,14] with the central N atom playing an important role in the process of heterolytic cleavage or formation of H_2. Because of the key function of the central N atom of ADT, some aromatic alkyl-functionalized ADT complexes have been synthesized as models of the active site.[9,11,15] However, as far as we know, systematic studies on the influence of different ADT bridges on diiron complexes are absent, and little attention has been paid to cycloalkyl-substituted ADT model compounds.

To further investigate the role of the ADT bridges in diiron complexes, and to develop the biomimetic chemistry of [FeFe]-hydrogenases, we have synthesized six (N-C_nH_{2n-1})-1,3-azapropanedithiolate-bridged diiron compounds (**1–6**) that bear typical structural similarities with the active site of [FeFe]-hydrogenases. In complexes **4–6**, PMe_3 was selected to substitute for the CO on the iron atoms to mimic the CN^--functionalized diiron complexes in nature. In this article, we will describe the coordination configurations, spectroscopic characterization, electrochemical properties and catalyzing mechanism of H_2 production processes promoted by complexes **1–6**.

Results and discussion

Synthesis of complexes 1–6

Complexes **1–3** were prepared in several steps according to literature procedures. Starting from $Fe_2S_2(CO)_6$,[16–18] we obtained $Fe_2(SH)_2(CO)_6$, which condensed with formaldehyde in the presence of primary amines (namely cyclopentylamine, cyclohexylamine and cycloheptylamine) to give the corresponding diiron complexes in 70–80% yield.[19,20] Disubstituted complexes (**4–6**) were synthesized in moderate yields by treating complexes **1–3** with PMe_3 in hexane, respectively.[5,21] The mixture was stirred for 24 h at room temperature under a nitrogen atmosphere until the color of the solution turned from red to purple. Single crystals suitable for X-ray analysis were obtained by extracting and subsequently recrystallizing from different freshly distilled solvents, namely pentane, hexane or heptane, in light of the solubilities of the products.

Molecular structures of complexes 1–6

The structures of the six compounds were unambiguously determined by X-ray diffraction, and their molecular diagrams are displayed in Fig. 1. Complexes **1–3** are (N-C_nH_{2n-1})-1,3-azapropanedithiolate (n = 5, 6, 7)-bridged all-carbonyl diiron complexes, while **4–6** are their PMe_3-disubstituted derivatives. There are two molecules per asymmetric unit cell,

[a] *Fujian Institute of Research on the Structure of Matter, Chinese Academy of Sciences, Fuzhou 350002, China. E-mail: ccn@fjirsm.ac.cn; Fax: +86 591/83792395; Tel: +86 591/83792395*
[b] *Department of Chemistry, Graduate University of Chinese Academy of Sciences, Beijing 100049, China*

† Electronic supplementary information (ESI) available: Selected bond lengths and angles. See DOI: 10.1039/b616236c

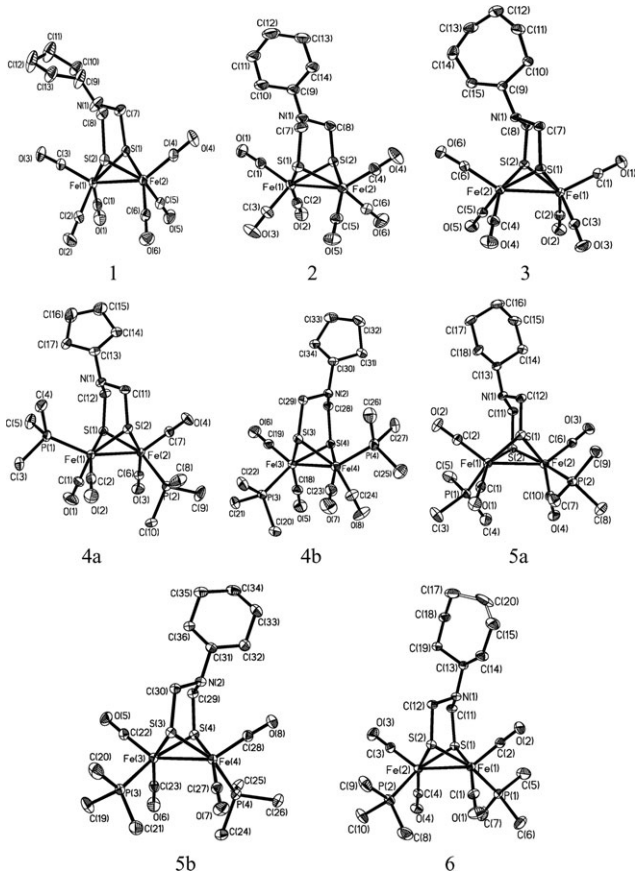

Fig. 1 Crystal structures of **1–6** (**4a** and **4b**, and **5a** and **5b** are two pairs of optical isomers of **4** and **5**, respectively).

representing the two different optical isomers in the crystal structures of both **4** and **5** (Fig. 1: **4a** and **4b** for **4**; **5a** and **5b** for **5**). In these structures, the 2Fe2S cores are all in a "butterfly" conformation, and each iron atom is coordinated in a pseudo square-pyramidal geometry. Each structure has two fused six-membered rings, one in the chair conformation and the other in the boat conformation. For example, in complex **1**, the N(1)C(7)S(1)Fe(2)S(2)C(8) ring is in the chair conformation while the N(1)C(7)S(1)Fe(1)S(2)C(8) ring in the boat conformation.

The cyclopentyl moiety in the crystal structure of **1** resides in a pseudo-equatorial position relative to the metalloheterocycle, while the cycloalkyl groups in the crystal structures of **2** and **3** are in axial positions. In the PMe_3-disubstituted complex **4**, one PMe_3 ligand is coordinated to an equatorial site on an iron atom, which is similar to the conformation of the benzyl-functionalized PMe_3-disubstituted complex $[(C_6H_5CH_2)N(SCH_2)_2Fe_2(CO)_4(PMe_3)_2]$ (**7**),[10,11] while complexes **5** and **6** feature a basal/basal configuration (Fig. 1). In addition, it is notable that the introduction of phosphine ligands may change the initial conformation of the substituted ADT bridges in their crystal structures. In complex **4**, the cyclopentyl moiety is not in a pseudo-equatorial but an axial position relative to the metalloheterocycle. The switch between equatorial and axial positions of the cyclopentyl ring upon phosphine substitution (**1** to **4**) could be explained by fluxionality of the ADT bridge in solution and the steric requirement of the substitution process, namely, sterically less crowded. This is the same reason for axial/basal phosphine orientation in the least sterically encumbered diphosphine complex **4** and basal/basal orientation in **5** and **6**.

Table 1 Fe–Fe bond lengths of complexes **1–6**, **8**, **9**, **10** and **11**

Complex	Fe–Fe bond/Å
1	2.5025(7)
2	2.5280(10)
3	2.5103(7)
4	2.5279(13)
5	2.6374(8)
6	2.6118(5)
8	2.5076
9	2.4924
10	2.554
11	2.5094

The Fe–Fe bonds in **4**, **5** and **6** (2.5279(13), 2.6374(8) and 2.6118(5) Å) are longer than those of their parent complexes **1**, **2** and **3** (2.5025(7), 2.5280(10) and 2.5103(7) Å), respectively, which is mainly caused by the introduction of PMe_3, which is a stronger electron-donating ligand than CO. The Fe–Fe bond lengths of **5** and **6** are also very close to those in the structures of enzymes from *Clostridium pasteurianum* and *Desulfovibrio desulfuricans* (*ca.* 2.6 Å).[12,13]

The Fe–Fe bond of **2** is the longest in those of **1**, **2** and **3**, and that of **5** is the longest in those of **4**, **5** and **6**. The reason for this is that the cyclohexyl group in **2** and **5** is a stronger electron donor than cyclopentyl or cycloheptyl. The cyclohexyl group makes the Fe atoms in **2** and **5** more electron rich and thus elongates the Fe–Fe bonds. Similarly, the Fe–Fe bond in **1** (2.5025(7) Å) is close in length to that of methoxyphenyl-functionalized all-carbonyl complex $[(\mu\text{-}SCH_2)_2N(C_6H_4OMe\text{-}p)Fe_2(CO)_6]$ (**8**) (2.5076 Å), while longer than that of Me-functionalized all-carbonyl compound $[(\mu\text{-}SCH_2)_2N(Me)Fe_2(CO)_6]$ (**9**) (2.4924 Å).[9] In addition, it has been reported that the Fe–Fe bond of PPh_3-substituted complex $[(\mu\text{-}SCH_2)_2N(C_6H_4OMe\text{-}p)Fe_2(CO)_5PPh_3]$ (**10**) (2.554 Å) is longer than that of its analogue $[(\mu\text{-}SCH_2)_2N(C_6H_4Br\text{-}p)Fe_2(CO)_5PPh_3]$ (**11**) (2.5094 Å) (Table 1).[22] These results suggest that the more strongly electron donating is the bridge, the longer the Fe–Fe bond is.

Spectroscopic characterization of complexes 1–6

Complexes **1–6** were characterized by elemental analysis, ^1H and ^{31}P NMR, and mass spectroscopy.

The mass spectra in API-ESI positive mode show the parent ion peaks at m/z 455.0 $[M + H]^+$ for **1**, 470.0 $[M + H]^+$ for **2**, 484.0 $[M + H]^+$ for **3**, 552.0 $[M + H]^+$ for **4**, 565.9 $[M + H]^+$ for **5** and 580.0 $[M + H]^+$ for **6**.

Owing to the electronic effects of the different cycloalkyl groups, the ^1H NMR signals of **2** are downfield-shifted compared to those of **1** and **3**. **1–3** each display a singlet for their CH_2S groups (δ = 3.301 for **1**, 3.385 for **2** and 3.226 for **3**). Influenced by the ADT N atoms, the nearest H (9-H) atoms of the cycloalkyl groups in **1–3** present themselves as singlets, respectively (δ = 3.009 for **1**, 2.470 for **2** and 2.522 for **3**), while the signals for the other H atoms on the cycloalkyl groups shift upfield (δ = 1.722–1.260 for **1**, 1.730–1.013 for **2**

Table 2 Comparison of ν(CO) bands in complexes **1–6**, **7**, **12** and **13**

Complex	ν(CO)/cm^{-1}	Notes
1	2069(s), 2025(s), 1989(s)	This work
2	2071(s), 2023(s), 1979(s)	This work
3	2072(s), 2033(s), 1993(s)	This work
4	1976(s), 1940(s), 1905(s)	This work
5	1966(m), 1940(s), 1901(s)	This work
6	2035(m), 1938(s), 1887(s)	This work
12	2074(m), 2036(s), 1995(s)	Refs. 6–8
13	1979(s), 1942(s), 1898(s)	Refs. 5–8
7	1980, 1943, 1892	Refs. 10 and 11

and 1.708–1.295 for **3**). The introduction of PMe_3 makes the signals of the CH_2S groups shift upfield and has little influence on the signals of the H atoms of the cycloalkyl groups. Interestingly, only a singlet in the ^{1}H NMR spectra for the PMe_3 group is observed for **4**, **5** and **6**, respectively, implying fast fluxionality of the PMe_3 ligand in solution.

The ^{31}P NMR spectra of **4–6** each show a singlet for their PMe_3 groups (δ = 29.935 for **4**, 24.108 for **5** and 24.085 for **6**), again indicating the fluxionality the PMe_3 group in solution. Because of a different conformation, the ^{31}P NMR signal of **4** is downfield-shifted compared to those of **5** and **6**.

We have studied the CO stretching frequency in the region 1880–2075 cm^{-1} for complexes **1–6**. The IR ν(CO) data of **1–6**, together with those of [(μ-PDT)$Fe_2(CO)_6$] (PDT = 1,3-propanedithiolate) (**12**), [(μ-PDT)$Fe_2(CO)_4$ $(PMe_3)_2$] (**13**) and [$Fe_2(CO)_4(PMe_3)_2(CH_2S)_2N$–$CH_2$–$C_6H_5$] (**7**), are listed in Table 2 for comparison.[5–8] Table 2 demonstrates that the introduction of two phosphine ligands lowers the CO stretching frequency, which indicates an enhancement of the electron density at the two iron atoms and a weakening of the CO triple bonds. The IR behavior described above resembles that displayed by previously reported PDT-bridged analogs.[20]

The average ν(CO) value of PDT-bridged all-carbonyl complex **12** is higher than those of **1**, **2** and **3** because cycloalkyl-substituted ADT bridges are better electron donors than PDT bridges.

The average ν(CO) values of **1** and **3** are higher than that of **2**. The cyclohexyl group enhances electron accumulation on the Fe atoms of **2**, leading to stronger back-bonding from the Fe atoms to CO and a weakening of the CO triple bonds.

In the subset of complexes **4**, **5**, **6**, **7** and **13**, each one has a wave number at or near 1940 cm^{-1}, suggesting PMe_3 has a characteristic influence on the CO stretching frequency. This means that the CO stretching frequency is influenced by both the ADT bridges and the ligand on the iron atoms, in particular the latter when it is a strong electron-donor.

Cyclic voltammograms of complexes 1–6

The cyclic voltammograms (CV) of complexes **1–6** were studied to evaluate the effects of different ADT bridges and PMe_3 on the redox properties of the iron cores of the model complexes. All the CV measurements were carried out in CH_3CN (with 0.1 M n-Bu_4NPF_6 as the electrolyte) and scanned in the cathodic direction, as indicated in Fig. 2 and Fig. 3. **1–3** display one quasi-reversible reduction, one irreversible reduction and two irreversible oxidation peaks, while **4–6** are manifested by two irreversible reduction and two irreversible oxidation peaks, respectively. The first reduction peaks at −1.663 V for **1**, −1.656 V for **2**, −1.685 V for **3**, −1.997 V for **4**, −1.993 V for **5** and −1.999 V for **6** are ascribed to the first one-electron reduction process from Fe^IFe^I to Fe^IFe^0, by comparison with electrochemical studies of other ADT-bridged diiron complexes.[9–11,21] Similarly, the second reduction peaks at −2.217 V for **1**, −2.240 V for **2**, −2.207 V for **3**, −2.316 V for **4**, −2.293 V for **5** and −2.351 V for **6**, are assigned to the one-electron reduction process from Fe^IFe^0 to Fe^0Fe^0. The first oxidation peaks of complexes **1–6**, 0.547, 0.588, 0.575, −0.212, −0.205 and −0.221 V, respectively, are ascribed to the one-electron oxidation process from Fe^IFe^I to Fe^IFe^{II}. The second oxidation peaks for complexes **1–6**, 0.879, 0.921, 0.903, −0.087, −0.0770 and −0.0777 V, respectively, are assigned to the second electron-transfer process from Fe^IFe^{II} to $Fe^{II}Fe^{II}$. Their electrochemical data, together with those of complexes [(μ-$SCH_2)_2N(C_6H_4OMe$-$p)Fe_2(CO)_6$] (**8**) and [(μ-$SCH_2)_2N(C_6H_4OMe$-$p)Fe_2(CO)_5PPh_2H$] (**14**), are given in Table 3.

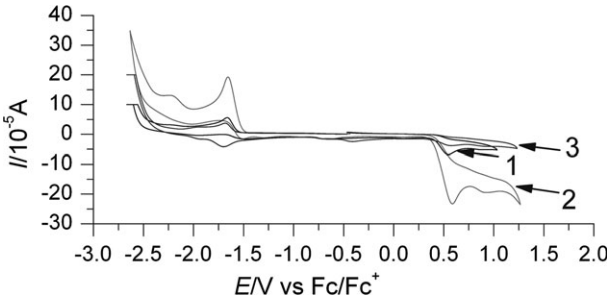

Fig. 2 Cyclic voltammograms of **1**, **2** and **3**.

Compared with the methoxyphenyl-functionalized all-carbonyl complex **8**, complexes **1–3** are reduced with more difficultly, indicating that the different electronic effects of the cycloalkyl and C_6H_4OMe-p groups result in different electron accumulations on the iron cores in each individual complex.

The CV data of complexes **4–6** are shifted in a cathodic direction compared to their parent complexes **1–3**, respectively. It is the stronger donor character of PMe_3 that renders the reduction of iron atoms more difficult. **4–6** are also reduced with more difficultly than **14**, resulting from both different phosphine ligands and different ADT bridges.

The reduction behaviours of complexes **2**, **3**, **5** and **6** were further studied by cyclic voltammetric techniques in the presence of HOAc. As shown in Fig. 4, after HOAc was added,

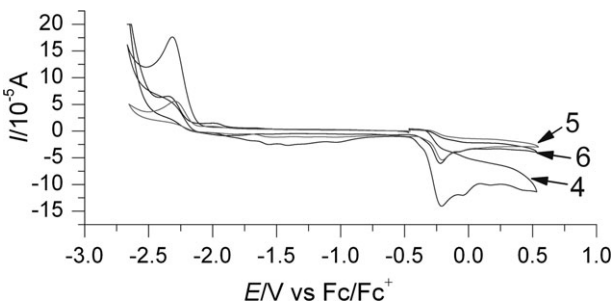

Fig. 3 Cyclic voltammograms of **4**, **5** and **6**.

Table 3 Electrochemical data of **1–6**, **8** and **14** (*vs.* Fc/Fc^+)

Complex	E_{pa}/V $Fe^IFe^I/Fe^{II}Fe^I$	E_{pa}/V $Fe^{II}Fe^I/Fe^{II}Fe^{II}$	E_{pc}/V Fe^IFe^I/Fe^0Fe^I	E_{pc}/V Fe^0Fe^I/Fe^0Fe^0
1	0.547	0.879	−1.663	−2.217
2	0.588	0.921	−1.656	−2.240
3	0.575	0.903	−1.685	−2.207
4	−0.212	−0.087	−1.997	−2.316
5	−0.205	−0.0770	−1.993	−2.293
6	−0.221	−0.0777	−1.999	−2.351
8	0.48	0.81	−1.61	−2.10
14	0.26	0.49	−1.78	−2.22

the first electrochemically irreversible one-electron reduction peak of **5** (−1.993 V *vs.* Fc/Fc^+) grew, but its position didn't shift. This indicated that H^+ was not attached to the model complex at that time, while the second reduction peak shifted to a more positive potential by 0.060 V after addition of one equiv. of HOAc to a 1 mM solution of **5**, implying that H^+ was introduced. Addition of a second equiv. of HOAc made the second reduction peak shift towards a more positive potential by another 0.077 V while the position of the first reduction peak did not shift. The addition of further acid led to the growth of the second reduction peak height, and caused its position to shift slightly to a more negative potential, indicating that excess H^+ didn't incorporate into the model complex. Complexes **2**, **3** and **6**, as shown in Fig. 5, had similar catalytic cycles to that of **5**. The observations described above are indicative of catalytic proton reduction. The catalytic activity of **5** was also supported by the electrolysis of a 1 mM solution of **5** (5 ml, 5 mM) with excess HOAc (20 mM) at −2.3 V. The initial rate of electrolysis was approximately 1.8 times that without **5**. 12 F mol^{-1} passed within 20 min, corresponding to 6 turnovers.

Based on the previously reported electrochemical behaviors of other diiron analogues[9,10,19,21,23] and the electrochemical data of our model complexes, we think an electrochemical–chemical–electrochemical–chemical (ECEC) mechanism is rational for the catalytic cycles of complexes **2**, **3**, **5** and **6** (Scheme 1). For example, **5** is firstly electrochemically reduced to $\mathbf{5}^-$ at its initial −1.993 V. Then, the reduced iron atom is protonated to form **5H**, which is followed by the second iron atom electrochemical reduction leading to $\mathbf{5H}^-$.

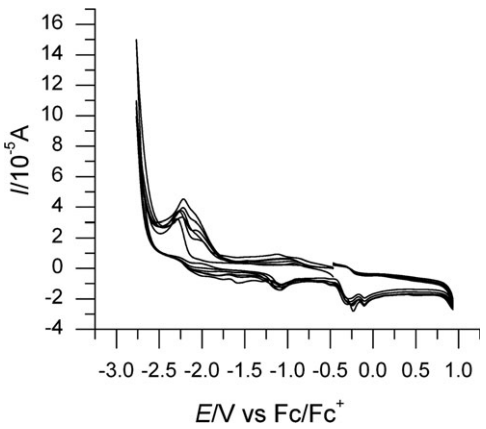

Fig. 4 Cyclic voltammogram of **5** (1.0 mM) with HOAc.

This transitional form is easily protonated, releasing H_2 and liberating the catalyst.

To the best of our knowledge, this is the first time the ECEC mechanism has been proposed for a H_2 production process catalyzed by mimics of [FeFe]-hydrogenases, which was initially proposed only for [NiFe]-hydrogenases.[23] This mechanism is different from the EECC mechanism[9] proposed for **8** and the CECE mechanism[11] suggested for $[(\mu\text{-}SCH_2)_2\text{-}N(C_6H_4Br\text{-}p)Fe_2(CO)_6]$ (**15**). In our case, because the ADT nitrogen atom was not protonated, the reduction potentials in the catalytic process were more negative than those in the similar process catalyzed by **15**. However, it may be the richer electron accumulation on the Fe atoms of our model complexes, caused by the cycloalkyl groups, that makes one Fe atom become protonated after the first electrochemical reduction, which is different from the EECC mechanism suggested for **8**. This indicates that the bridge influences the mechanism of catalytic proton reduction.

Experimental section

General procedures

All reactions were carried out under dry, oxygen-free nitrogen using standard Schlenk techniques. Solvents were dried and distilled prior to use according to standard methods. Commercially available chemicals such as paraformaldehyde, $Fe(CO)_5$, PMe_3 (1 M in THF), $LiBEt_3H$, F_3CCOOH and $C_nH_{2n-1}NH_2$ (n = 5, 6, 7) were reagent grade and used as received. The starting complex $[Fe_2S_2(CO)_6]$ was prepared according to the literature.[16–18] Elemental analysis was carried out on a Vario EL III Elemental Analyser. IR spectra were taken on a Magna-75 FT-IR spectrophotometer using KBr pellets in the range of 4000–400 cm^{-1}. ^1H NMR spectra were collected on a Varian Unity 500NMR spectrometer. Mass spectra were recorded on an DECAX-3000 LCQ Deca XP instrument.

Synthesis of $[Fe_2(CO)_6(CH_2S)_2N\text{–}C_5H_9]$ (1). $Fe_2S_2(CO)_6$ (1 mM, 0.344 g) was dissolved in dry THF (40 ml) under a nitrogen atmosphere and then cooled to −78 °C with acetone and liquid nitrogen. After the solution was stirred for 30 min, $LiBEt_3H$ (2 mM) was added dropwise very slowly. At the midpoint of the addition, the color of the reaction mixture turned from red to dark green; for the rest of addition it remained green. After another 30 min, F_3CCOOH (2 mM, 0.149 ml) was added. The new mixture was stirred for an additional hour. The cool solution was added to a mixture of paraformaldehyde (40 mM,

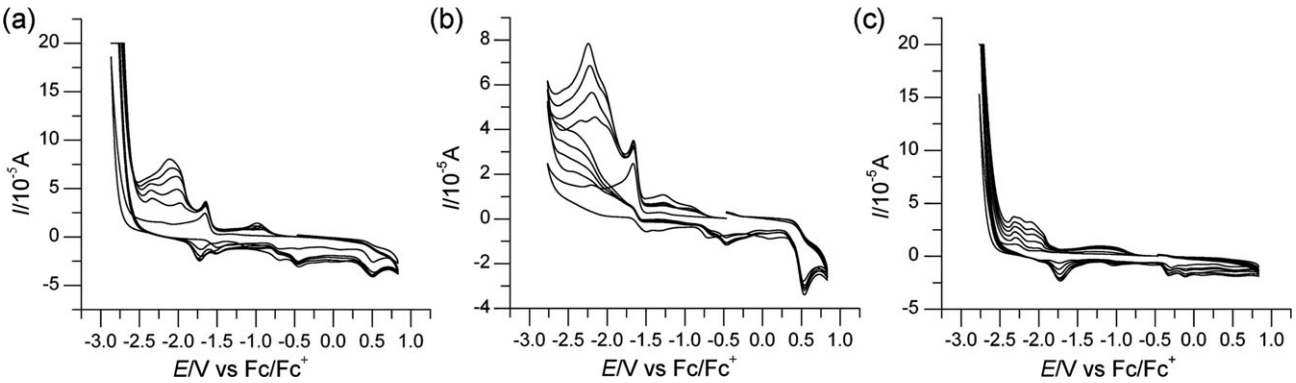

Fig. 5 Cyclic voltammograms of (a) **2**, (b) **3** and (c) **6** (1.0 mM) with HOAc.

1.2 g) and $C_5H_9NH_2$ (1 mM, 1.98 ml) in THF that had been stirred for 10 h and cooled to 0 °C. The combined mixture was stirred for 24 h and the majority of the solvent was evaporated under vacuum.[19] The remaining solution was filtered through silica gel. A red fraction was collected by elution with hexane. Recrystallization of the crude product from freshly distilled pentane in a fridge at −20 °C for several days gave compound **1** (0.342 g, 75%) as dark red crystals (found: C, 34.33; H, 2.89; N, 3.10. Calc. for $C_{13}H_{13}Fe_2S_2O_6N$: C, 34.31; H, 2.88; N, 3.08%); δ_H (500 MHz; $CDCl_3$; Me_4Si): 3.301 (4H, s, $2CH_2S$), 3.009 (1H, s, 9-H), 1.722–1.260 (8H, m, $4CH_2$); *m*/*z* 455.0 (49%, M + H^+).

Synthesis of $[Fe_2(CO)_6(CH_2S)_2N–C_6H_{11}]$ (2). Compound **2** was prepared using a procedure similar to that used for preparing **1**, except that $C_6H_{11}NH_2$ (1 mM, 2.24 ml) was used as the primary amine. Recrystallization of the crude product from freshly distilled hexane gave compound **2** (0.37 g, 80%) as red crystals (Found: C, 35.90; H, 3.19; N, 2.88. Calc. for $C_{14}H_{15}Fe_2S_2O_6N$: C, 35.85; H, 3.22; N, 2.99%); δ_H (500 MHz; $CDCl_3$; Me_4Si): 3.385 (4H, s, $2CH_2S$), 2.470 (1H, s, 9-H), 1.730–1.013 (10H, m, $5CH_2$); *m*/*z* 470.0 (100%, M + H^+).

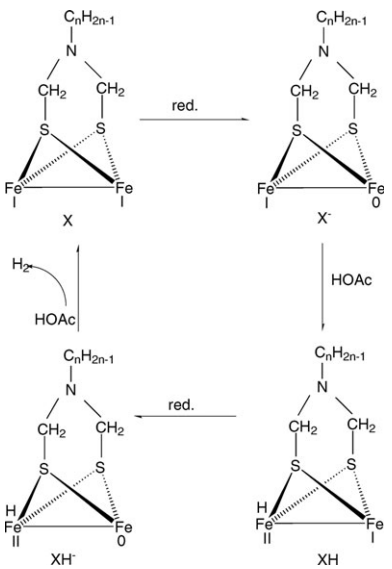

Scheme 1 ECEC mechanism proposed for the H_2 production process catalyzed by our complexes (X = **2**, **3**, **5** or **6**).

Synthesis of $[Fe_2(CO)_6(CH_2S)_2N–C_7H_{13}]$ (3). Compound **3** was prepared using a procedure similar to that used for preparing **1**, except that $C_7H_{13}NH_2$ (1 mM, 3.00 ml) was used as the primary amine. Recrystallization of the crude product from freshly distilled heptane in a fridge at −20 °C for several days gave compound **3** (0.34 g, 70%) as dark red crystals (Found: C, 37.10; H, 3.44; N, 2.99. Calc. for $C_{15}H_{17}Fe_2S_2O_6N$: C, 37.29; H, 3.55; N, 2.90%); δ_H (500 MHz; $CDCl_3$; Me_4Si): 3.226 (4H, s, $2CH_2S$), 2.522 (1H, s, 9-H), 1.708–1.295 (12H, m, $6CH_2$); *m*/*z* 484.0 (100%, M + H^+).

Synthesis of $[Fe_2(CO)_4(PMe_3)_2(CH_2S)_2N–C_5H_9]$ (4). PMe_3 (2 mM, 2 ml) was added to a solution of complex **1** (0.228 g, 0.5 mM) in 10 ml of freshly distilled hexane under a nitrogen atmosphere. After 24 h of stirring, the color of the solution changed from red to purple. The solvent and unreacted PMe_3 were then removed under vacuum. The resulting dark brown residue was extracted with toluene and recrystallized from freshly distilled pentane to give **4** (0.166 g, 60%) as dark red crystals (Found: C, 37.10; H, 5.58; N, 2.49. Calc. for $C_{17}H_{31}Fe_2S_2O_4NP_2$: C, 37.04; H, 5.67; N, 2.54%); δ_H (500 MHz; $CDCl_3$; Me_4Si): 3.190 (4H, s, $2CH_2S$), 2.830 (1H, s, 13-H), 1.782–0.868 (8H, m, $4CH_2$), 1.259 (18H, s, $2PMe_3$); δ_P (202 MHz; $CDCl_3$; Me_4Si): 29.935 (PMe_3); *m*/*z* 552.0 (100%, M + H^+).

Synthesis of $[Fe_2(CO)_4(PMe_3)_2(CH_2S)_2N–C_6H_{11}]$ (5). Compound **5** was prepared using a procedure similar to that used for preparing **4**, except that $[Fe_2(CO)_6S_2(CH_2)_2N–C_6H_{11}]$ (0.235 g, 0.5 mM) was used as the starting all-carbonyl complex. The resulting dark brown residue was extracted with toluene, followed by a recrystallization from freshly distilled hexane to give **5** (0.164 g, 58%) as dark red crystals (Found: C, 38.10; H, 5.78; N, 2.49. Calc. for $C_{18}H_{33}Fe_2S_2O_4NP_2$: C, 38.25; H, 5.88; N, 2.48%); δ_H (500 MHz; $CDCl_3$; Me_4Si): 3.245 (4H, s, $2CH_2S$), 2.370 (1H, s, 13-H), 1.700–1.011 (10H, m, $5CH_2$), 1.482 (18H, s, $2PMe_3$); δ_P (202 MHz; $CDCl_3$; Me_4Si): 24.108 (PMe_3); *m*/*z* 565.9 (100%, M + H^+).

Synthesis of $[Fe_2(CO)_4(PMe_3)_2(CH_2S)_2N–C_7H_{13}]$ (6). Compound **6** was prepared using a procedure similar to that used for preparing **4**, except that $[Fe_2(CO)_6S_2(CH_2)_2N–C_7H_{13}]$ (0.241 g, 0.5 mM) was used as the starting all-carbonyl complex. The resulting brown residue was extracted with toluene, followed by a recrystallization from freshly distilled

Table 4 Crystallographic data summary for complexes **1–6**[a]

	1	2	3	4	5	6
Empirical formula	$C_{13}H_{13}Fe_2NO_6S_2$	$C_{14}H_{15}Fe_2NO_6S_2$	$C_{15}H_{17}Fe_2NO_6S_2$	$C_{17}H_{31}Fe_2NO_4P_2S_2$	$C_{18}H_{33}Fe_2NO_4P_2S_2$	$C_{19}H_{35}Fe_2NO_4P_2S_2$
Formula weight	455.06	469.09	483.12	551.19	565.22	579.24
Space group	$P2(1)/n$	$P2(1)/c$	$P2(1)/n$	$P\bar{1}$	$P2(1)/c$	$P2(1)/n$
a/Å	7.7471(9)	9.6577(2)	10.604(3)	12.4237(5)	22.819(5)	11.0584(6)
b/Å	11.7596(15)	13.08730(10)	12.035(4)	14.1988(6)	10.912(2)	22.4454(10)
c/Å	19.604(2)	14.9696(2)	15.428(4)	14.6021(6)	23.588(5)	11.6423(6)
α/°	90	90	90	98.3330(10)	90	90
β/°	90.778(5)	92.7930(10)	92.439(6)	91.9110(10)	118.581(2)	113.615(2)
γ/°	90	90	90	94.4710(10)	90	90
V/Å^3	1785.8(4)	1889.81(5)	1967.2(10)	2538.28(18)	5158.0(19)	2647.7(2)
Z	4	4	4	8	8	4
ρ_{calc}/g cm^{-3}	1.693	1.649	1.631	1.442	1.456	1.453
λ(Mo-K$_\alpha$)/Å	0.71073	0.71073	0.71073	0.71073	0.71073	0.71073
T/K	293(2)	293(2)	293(2)	293(2)	293(2)	293(2)
μ/mm^{-1}	1.885	1.784	1.717	1.454	1.433	1.398
R^b	0.0480	0.0521	0.0310	0.0785	0.0568	0.0410
wR^c	0.0928	0.1259	0.0894	0.2815	0.0973	0.1335

[a] CCDC reference numbers 622703–622708. For crystallographic data in CIF or other electronic format see DOI: 10.1039/b616236c. [b] $R = \sum||F_o| - |F_c||/\sum|F_o|$. [c] $wR = [\sum w(|F_o| - |F_c|)^2/\sum wF_o^2]^{\frac{1}{2}}$.

heptane to give **6** (0.144 g, 50%) as dark red crystals (Found: C, 39.35; H, 6.10; N, 2.49. Calc. for $C_{19}H_{35}Fe_2S_2O_4NP_2$: C, 39.40; H, 6.09; N, 2.42%); δ_H (500 MHz; $CDCl_3$; Me_4Si): 3.129 (4H, s, $2CH_2S$), 2.426 (1H, s, 13-H), 1.700–0.866 (12H, m, $6CH_2$), 1.488 (18H, s, $2PMe_3$); δ_P (202 MHz; $CDCl_3$; Me_4Si) 24.085 (PMe_3); m/z 580.0 (100%, M + H$^+$).

X-Ray structure determination of complexes 1–6. Single crystals of complexes **2** and **4** were mounted on a Siemens Smart CCD diffractometer with Mo-K$_\alpha$ radiation (λ = 0.71073 Å). Single crystals of complexes **1**, **3**, **5** and **6** were performed on a Mercury-CCD diffractometer equipped with graphite-monochromated Mo-K$_\alpha$ radiation (λ = 0.71073 Å). All data were collected at 293(2) K using a ω-2θ scanning mode. An empirical absorption correction was made of the multi-scan type. The structure was solved by direct methods and refined by full-matrix least-squares techniques using the SHELXL-97 program.[24] Anisotropic displacement parameters were refined for all non-hydrogen atoms. The hydrogen atoms were added in a riding model and not refined. Crystallographic data of **1–6** are outlined in Table 4.

Electrochemistry

Acetonitrile (Aldrich Chemicals, spectroscopy grade) was the solvent used for the electrochemistry, with a solution of 0.1 M n-Bu_4NPF_6 in MeCN being used as the electrolyte. The electrolyte solution was de-gassed by bubbling argon through it for 10 min before measurements were carried out. All electrochemistry results were obtained at a scan rate of 100 mV s^{-1} by using a CHI660A potentiostat and a three-electrode cell under argon. The working electrode was a glassy carbon disc (diameter 3 mm) polished with 1 μm diamond pastes and sonicated in ion-free water for 10 min. The reference electrode was a Ag/AgCl electrode (3 M KCl in H_2O) and the auxiliary electrode was a platinum wire. All potential data are quoted against the Fc/Fc$^+$ potential.

Conclusions

Selecting an appropriate ADT bridge is important for obtaining a good mimic of the active site of [FeFe]-hydrogenases, which can reduce protons to H_2 at a relatively high potential. The electronic effect of the ADT is a key factor on the redox properties of the model diiron complex because the bridge influences the H_2 production mechanism.

Acknowledgements

We are grateful to the National Key Foundation of China (no. 20633020), the Science & Technology Innovation Foundation for the Young Scholar of Fujian Province (no. 2005J059), and the National Nature Science Foundation of China (no. 20471061) for their financial support of this work.

References

1 (*a*) M. Y. Darensbourg, E. J. Lyon and J. J. Smee, *Coord. Chem. Rev.*, 2000, **206–207**, 533–561; (*b*) M. Y. Darensbourg, E. J. Lyon, X. Zhao and I. P. Georgakaki, *Proc. Natl. Acad. Sci. U. S. A.*, 2003, **100**, 3683–3688; (*c*) D. J. Evans and C. J. Pickett, *Chem. Soc. Rev.*, 2003, **32**, 268–275; (*d*) X. Liu, S. K. Ibrahim, C. Tard and C. J. Pickett, *Coord. Chem. Rev.*, 2005, **249**, 1641–1652.
2 (*a*) M. Frey, *ChemBioChem*, 2002, **3**, 153–160; (*b*) S. P. J. Albracht, *Biochem. Acta*, 1994, **1188**, 167–204; (*c*) A. Volbeda, M. H. Charon, C. Piras, E. C. Hatchikian, M. Frey and J. C. Fontecilla-Camps, *Nature*, 1995, **373**, 580–587; (*d*) R. Cammack, *Nature*, 1999, **397**, 214–215; (*e*) M. W. W. Adams and E. I. Stiefel, *Science*, 1998, **282**, 1842–1843; (*f*) J. Alper, *Science*, 2003, **299**, 1686–1687.
3 M. Korbas, S. Vogt, W. Meyer-Klaucke, E. Bill, E. J. Lyon, R. K. Thauer and S. Shima, *J. Biol. Chem.*, 2006, **281**, 30804–30813.
4 M. W. W. Adams, *Biochim. Biophys. Acta*, 1990, **1020**, 115–145.
5 L. Schwartz, G. Eilers, L. Eriksson, A. Gogoll, R. Lomoth and S. Ott, *Chem. Commun.*, 2006, 520–522.
6 X. Zhao, I. P. Georgakaki, M. L. Miller, J. C. Yarbrough and M. Y. Darensbourg, *J. Am. Chem. Soc.*, 2001, **123**, 9710–9711.
7 E. J. Lyon, I. P. Georgakaki, J. H. Reibenspies and M. Y. Darensbourg, *Angew. Chem., Int. Ed.*, 1999, **38**, 3178–3180.
8 D. Chong, I. P. Georgakaki, R. Mejia-Rodriguez, J. Sanabria-Chinchilla, M. P. Soriaga and M. Y. Darensbourg, *Dalton Trans.*, 2003, 4158–4163.
9 L.-C. Song, J.-H. Ge, X.-G. Zhang, Y. Liu and Q.-M. Hu, *Eur. J. Inorg. Chem.*, 2006, 3204–3210.

10 S. Ott, M. Kritikos, B. Åkermark, L.-C. Sun and R. Lomoth, *Angew. Chem., Int. Ed.*, 2004, **43**, 1006.
11 S. Ott, M. Kritikos, B. Åkermark and L.-C. Sun, *Angew. Chem.*, 2003, **115**, 3407–3410.
12 Y. Nicolet, C. Piras, P. Legrand, E. C. Hatchikian and J. C. Fontecilla-Camps, *Structure*, 1999, **7**, 13–23.
13 J. W. Peters, W. N. Lanzilotta, B. J. Lemon and L. C. Seefeldt, *Science*, 1998, **282**, 1853–1858.
14 Y. Nicolet, B. J. Lemon, J. C. Fontecilla-Camps and J. W. Peters, *Trends Biochem. Sci.*, 2000, **25**, 138–143.
15 H. Fan and M. B. Hall, *J. Am. Chem. Soc.*, 2001, **123**, 3828–3829.
16 D. Seyferth, R. S. Henderson and L.-C. Song, *Organometallics*, 1982, **1**, 125–133.
17 J. D. Lawrence, H. Li and T. B. Rauchfuss, *Chem. Commun.*, 2001, 1482–1483.
18 D. Seyferth and R. S. Henderson, *J. Organomet. Chem.*, 1981, **218**, C34–C36.
19 H.-X. Li and T. B. Rauchfuss, *J. Am. Chem. Soc.*, 2002, **124**, 726–727.
20 P. Li, M. Wang, C.-J. He, G.-H. Li, X.-Y. Liu, C.-N. Chen, B. Åkermark and L.-C. Sun, *Eur. J. Inorg. Chem.*, 2005, 2506–2513.
21 W. Dong, M. Wang, X.-Y. Liu, K. Jin, G.-H. Li, F.-J. Wang and L.-C. Sun, *Chem. Commun.*, 2006, 305–307.
22 S. Ott, M. Borgström, M. Kritikos, R. Lomoth, J. Bergquist, B. Åkermark, L. Hammarström and L. Sun, *Inorg. Chem.*, 2004, **43**, 4683–4692.
23 A. Perra, E. S. Davies, J. R. Hyde, Q. Wang, J. McMaster and M. Schröder, *Chem. Commun.*, 2006, 1103–1105.
24 G. M. Sheldrick, *SHELXL-97, Program for the refinement of crystal structures*, University of Göttingen, Germany, 1997.

